Published in final edited form as:
Am J Physiol Renal Physiol. 2008 April ; 294(4): F971–F981. doi:10.1152/ajprenal.00313.2007.

Heterogeneity of muscarinic receptor-mediated Ca^{2+} responses in cultured urothelial cells from rat

F. Aura Kullmann[1], **D. Artim**[1], **J. Beckel**[1,2], **S. Barrick**[1], **W. C. de Groat**[1], and **L. A. Birder**[1,2]

[1]Departments of Pharmacology, University of Pittsburgh School of Medicine, Pittsburgh, Pennsylvania

[2]Departments of Medicine, University of Pittsburgh School of Medicine, Pittsburgh, Pennsylvania

Abstract

Muscarinic receptors (mAChRs) have been identified in the urothelium, a tissue that may be involved in bladder sensory mechanisms. This study investigates the expression and function of mAChRs using cultured urothelial cells from the rat. RT-PCR established the expression of all five mAChR subtypes. Muscarinic agonists acetylcholine (ACh; 10 μM), muscarine (Musc; 20 μM), and oxotremorine methiodide (OxoM; 0.001–20 μM) elicited transient repeatable increases in the intracellular calcium concentration ($[Ca^{2+}]_i$) in ~50% of cells. These effects were blocked by the mAChR antagonist atropine methyl nitrate (10 μM). The sources of $[Ca^{2+}]_i$ changes included influx from external milieu in 63% of cells and influx from external milieu plus release from internal stores in 27% of cells. The use of specific agonists and antagonists (10 μM M_1 agonist McN-A-343; 10 μM M_2, M_3 antagonists AF-DX 116, 4-DAMP) revealed that M_1, M_2, M_3 subtypes were involved in $[Ca^{2+}]_i$ changes. The PLC inhibitor U-73122 (10 μM) abolished OxoM-elicited Ca^{2+} responses in the presence of the M_2 antagonist AF-DX 116, suggesting that M_1, M_3, or M_5 mediates $[Ca^{2+}]_i$ increases via PLC pathway. ACh (0.1 μM), Musc (10 μM), oxotremorine sesquifumarate (20 μM), and McN-A-343 (1 μM) acting on M_1, M_2, and M_3 mAChR subtypes stimulated ATP release from cultured urothelial cells. In summary, cultured urothelial cells express functional M_1, M_2, and M_3 mAChR subtypes whose activation results in ATP release, possibly through mechanisms involving $[Ca^{2+}]_i$ changes.

Keywords

bladder; Fura-2 calcium imaging; ATP

Overactive bladder conditions, occurring in pathologies, such as spinal cord injury (SCI) or in the elderly, represent major health problems which affect more than 17 million people worldwide. The standard treatment is antimuscarinic drugs which block muscarinic acetylcholine receptors (mAChRs) located on bladder smooth muscle. These receptors are activated by acetylcholine (ACh) released from parasympathetic efferent nerves during voiding (15,18). Antimuscarinic treatment decreases the frequency of voiding and, more importantly, decreases the number and severity of urge episodes (18). This suggests an action of antimuscarinics on bladder sensory pathways, such as a block of mAChRs in the urothelium and/or in the afferent nerves (18).

Address for reprint requests and other correspondence: F. Aura Kullmann, Dept. of Pharmacology, Univ. of Pittsburgh School of Medicine, E 1340 Biomedical Science Tower, Pittsburgh, PA 15261 (flnst2@pitt.edu).

The urothelium, a specialized epithelial tissue lining the urinary tract, is thought to play an important role in bladder function in normal as well as in pathological conditions (5,8). Several studies showed that the urothelium expresses a variety of receptors including muscarinic (13), nicotinic (2), purinergic (32), and transient receptor potential (TRPs) (8), which can detect mechanical or chemical changes in the environment. Activation of these receptors can trigger release of transmitters including ATP (7,17), nitric oxide (NO) (6), or ACh (25,58), which could act on urothelial cells and/or on afferent sensory nerves or efferent nerves located in the urothelium and suburothelium (20,23) and thus could contribute to bladder sensations such as fullness and pain (14,55).

A series of studies indicated that all subtypes (M_1–M_5) of mAChRs are expressed in the urothelium of several species. These studies used receptor binding assays, mRNA, and/or Western blot assays and immunostaining to demonstrate mAChRs expression in rat, mouse, pig, human urothelium and urothelial cell lines (10,13,21,22,28,33,34,59) (for a review, see Ref. 13). Some of these studies have also found that the distribution of mAChR subtypes was different in different layers of the urothelium (10,59). In mouse and human, M_1 mAChRs were found mostly in the basal plasma membrane of the basal cells, M_2 mAChRs appeared restricted to the umbrella cells while M_3, M_4, M_5 mAChRs were found distributed throughout the urothelium (10,59). Such a selective distribution may indicate distinct functions of these receptors that might be achieved through mAChR subtype-specific interactions with afferent and/or efferent urothelial and suburothelial nerves.

There is increasing evidence that urothelial mAChRs have an impact on bladder functions. In bladder strips from pig (26) and human (12), activation of urothelial mAChRs releases a diffusible factor which inhibits carbachol-induced smooth muscle contractions (12,26). In rat bladder in vitro, focal application of carbachol induces Ca^{2+} waves originating in the urothelium and suburothelial space (27), further supporting the involvement of these receptors in distinct aspects of bladder function. Also, recent data from our laboratory showed that in SCI cats and in normal rats, in vivo activation of urothelial mAChRs by intravesical administration of the muscarinic agonist oxotremorine methiodide (OxoM) alters reflex bladder contractions (30,52). However, the mechanisms of action and the subtypes of receptors involved are not well understood.

Given the wide use of antimuscarinic drugs in the treatment of overactive bladder and the increasing evidence that the urothelium is a major player in bladder sensations, this study sought to investigate the expression and function of urothelial mAChRs using cultured urothelial cells from rat. The results provide evidence for the expression of all mAChR subtypes and demonstrate that certain subtypes regulate intracellular Ca^{2+} levels and trigger release of ATP. These data provide support for the proposed role of urothelial mAChRs in bladder function and for interactions between urothelium (via urothelium-derived factors), efferent and afferent nerves, that together can modulate bladder activity.

Preliminary findings have been published in abstract form: Negoita (Kullmann) et al., Experimental Biology 2006.

Materials and Methods

Experimental animals

Tissue was removed from adult female Sprague-Dawley rats (200–250 g; Harlan, Indianapolis, IN). Care and handling of the animals have been approved by the University of Pittsburgh Institutional Animal Care and Use Committee.

Rat urothelial cell cultures were prepared as previously described (6). Female rats (200–250 g) were killed by CO_2 inhalation, and the bladder was removed and placed in cold minimal essential medium (MEM; Invitrogen, Carlsbad, CA) supplemented with HEPES (2.5 g/l; Sigma, St. Louis, MO) and containing penicillin/streptomycin/fungizone (PSF; 1%; Sigma). The bladder was cut open to expose the urothelium and incubated in dispase (2.5 mg/ml; Worthington Biochemical, Lakewood, NJ) overnight at 4°C. Urothelial cells were gently scraped from the underlying tissue, placed in trypsin (0.25% wt/vol; Sigma) for 10–15 min at 37°C, and dissociated by trituration. Cells were suspended in MEM containing 10% FBS (Invitrogen) and centrifuged at 416 *g* for 10 min. The supernatant was removed and cells were suspended in keratinocyte media (Invitrogen) with 1% PSF, centrifuged again, and resuspended in fresh media. Cells were plated on collagen-coated glass coverslips at densities of 50–125 × 10^4 cells/ml. Media were added after 4 h of incubation at 37°C and changed every other day. Cells were used 48–96 h after dissociation.

To prepare photomicrographs of cultured urothelial cells (Fig. 1, A–I), coverslips were washed with HBSS and placed in a petri dish with glass bottom. Images of live cells were taken with an inverted Olympus IX71 microscope equipped with ×10 and ×40 objectives using phase contrast. Since these cells are flat, the illumination was adjusted manually to an optimum for each field of view. Pictures were taken from cells after *days 2* to *6* in culture because on the first day in culture cells were not well attached and were washed away when changing media.

Immunocytochemistry

Cultured cells (from 2 and 4 days in culture) were fixed using 4% paraformaldehyde (~30 min), rinsed with PBS, incubated with blocking media (0.2% Triton X-100 and 5% donkey serum) for 2 h at room temperature (RT), and incubated in the primary antibody (Table 1) overnight at 4°C. The following day, coverslips were washed with PBS and incubated in secondary antibodies (Table 1) for 2 h at RT. Controls included omission of primary or secondary antibodies. No detectable staining was found in these coverslips. Cell nuclei were stained using DAPI (1:10,000 in PBS for 5 min; Invitrogen). Coverslips were mounted on microscope slides and images were taken with an inverted Olympus IX71 microscope equipped with a ×40 objective and a Hamamatsu digital camera controlled by the program C-Imaging (Compix, Cranberry Township, PA). Figures were prepared in Photoshop (Adobe Systems, San Jose, CA).

RNA extraction and quantitative RT-PCR

RNA was extracted from cultured cells (2–6 days after plating) or from urothelial tissue gently teased away from the remainder of the bladder using fine forceps and scissors. Cells or tissues were homogenized in TRIzol reagent (Life Technologies, Grand Island, NY) and RNA was extracted as per manufacturer's directions. Extracted RNA was resuspended in 50 μl of molecular grade water (RNase and DNase-free) and quantified using a UV-vis spectrophotometer. Qiagen's Omniscript RT kit (Qiagen, Chatsworth, CA) was used for the reverse transcriptase reaction, following the manufacturer's instructions and using 1 μg of RNA. For real-time quantitative PCR, 2 μl of either the RT reaction or a 10× or 100× dilution of the RT reaction were used with Bio-Rad's iQ SYBR Green Supermix. Real-time reactions were run in triplicate in Bio-Rad's MyiQ single color real-time thermal cycler and real-time data collected by computer. Primers for the PCR reaction were as follows: M_1: (L) CCTAGCATGGCTGGTTTCCT (R) GACCGTGACAGGGAGGTAGA; M_2: (L) TGCCTCCGTTATGAATCTCC (R) TCCACAGTCCTCACCCCTAC; M_3: (L) GTGCCATCTTGCTAGCCTTC (R) TCACACTGGCACAAGAGGAG; M_4: (L) GACGGTGCCTGATAACCAGT (R) CTCAGGTCGATGCTTGTGAA; and M_5: (L) CAGAGAAGCGAACCAAGGAC (R) CTCAGCCTTTTCCCAGTCAG.

Following the PCR reaction, the amplified products were subjected to a melting curve test. Amplification efficiencies were also calculated for each set of dilutions using the following equation: E = 10[−1/slope] (38). Real-time signals were considered to be indicative of correctly amplified products if: *1*) the melt curve analysis exhibited only one peak, *2*) amplification efficiencies were between 90 and 110%, and *3*) negative RT reactions as a negative control yielded no signal in real-time PCR. Samples from each well were also run on a SYBR Safe-stained agarose gel following PCR to confirm that each product was of the correct size and free from nonspecific products. Relative expression of the muscarinic subunits was then determined by normalizing to the lowest expressing subunit, M_4, using a method similar to Pfaffl (38). Relative expression values were averaged from results from four cultures from four animals.

Calcium imaging

Urothelial cells were loaded with 5 μM fura-2 AM (Molecular Probes, Eugene, OR) for 30 min at 37°C in an atmosphere of 5% CO_2. Fura-2 AM was dissolved in bath solution containing HBSS; in mM: 138 NaCl, 5 KCl, 0.3 KH_2PO_4, 4 $NaHCO_3$, 2 $CaCl_2$, 1 $MgCl_2$, 10 HEPES, 5.6 glucose, pH 7.4, 310 mosM/l to which BSA was added (5 mg/ml; Sigma) to promote loading. Coverslips were placed on an inverted epifluorescence microscope (Olympus IX70) or on upright microscope (Olympus BX61WI) and continuously superfused with HBSS (1.5–2 ml/min); in some experiments supplemented with 10 μM Trolox (Sigma) to diminish the effects of photobleaching (41). In both set-ups, drugs were bath applied through gravity-driven perfusion systems (flow rate 1.5–2 ml/min) by manually switching a valve from the container containing HBSS to the container containing the drug dissolved at the desired concentration. In the set-up equipped with the inverted microscope, the perfusion inlet was placed in close proximity to the imaged cells while in the set-up equipped with the upright microscope the perfusion inlet was placed at one side of the bath due to space constraints. Although there was a difference in the time necessary for the drug to reach the cells in the two systems (perfusion systems differed in the length of the perfusion tubing and in the placement of the perfusion inlet relative to the imaged cells), for data analysis $[Ca^{2+}]_i$ changes were measured in a time window of 30 s after the drug was estimated to reach the bath. Peak amplitude of $[Ca^{2+}]_i$ changes had to exceed two SD above the baseline to be considered drug-induced responses. To ensure that the results obtained in both set-ups were comparable, control experiments were performed on the two set-ups to measure the percentage of cells responding to 20 μM OxoM (46.8%; 128/273 cells vs. 42.3%; 36/85 cells), rise time (37.2 ± 1.6 s, n = 126 vs. 39.2 ± 1.4 s, n = 36; unpaired t-test, $P > 0.05$), and amplitude of the responses (37.9 ± 3.6% ΔR/R, n = 128 vs. 31.1 ± 3.1% ΔR/R, n = 36; unpaired t-test, $P > 0.05$). Fura-2 Ca^{2+} imaging was performed as previously described (16). In brief, fura-2 was excited alternately with UV light at 340 and 380 nm and the fluorescence emission was detected at 510 nm using a computer-controlled monochromator. Image pairs were acquired every 1 to 30 s using illumination periods between 20 and 50 ms. Wavelength selection, timing of excitation, and acquisition of images were controlled using C-Imaging software (Compix) running on a PC. Digital images were stored on a hard disk for off-line analysis.

Data analysis

Image analysis was performed using the program C-Imaging (Compix). Background was subtracted to minimize camera dark noise and tissue autofluorescence. An area of interest was drawn around each cell and the average value of all pixels included in this area was taken as one measurement. Data analysis was further performed using Excel (Microsoft, Redmond, WA) and Origin version 7 (OriginLab, Northampton, MA). Baseline $[Ca^{2+}]_i$ was determined from the average of five to eight measurements obtained before drug application. Amplitudes of Ca^{2+} responses were computed as the difference between the peak value and

the baseline value. Only cells responding to ATP (10–100 μM; >95% of urothelial cells responded to ATP), which was used as a control in each experiment were included in analysis. F.A.U. represents fluorescence arbitrary units and R is the ratio of fluorescence signal measured at 340 nm (F_{340nm}) divided by the fluorescence signal measured at 380 nm (F_{380nm}). The results are given as changes in R (F_{340nm}/F_{380nm}) before and after drug application (ΔR) and as percentage increase of R above baseline levels of $[Ca^{2+}]_i$ (ΔR/R).

To analyze the OxoM dose-response curve, data were fitted using Origin with the logistic function $y = A_2 + (A_1 - A_2)/1+(x/x_0)^p$, where x_0 is center (or EC_{50}), p is power (or Hill coefficient), A_1 is initial *y* value, A_2 is final *y* value. The *y* value at x_0 is half-way between the two limiting values A_1 and A_2: $y(x_0) = (A_1+A_2)/2$.

ATP release from cultured urothelial cells was performed as previously described (7). Coverslips containing urothelial cells were superfused with oxygenated Krebs (in mM: 4.8 KCl, 120 NaCl, 1.1 $MgCl_2$, 2.0 $CaCl_2$, 11 glucose, 10 HEPES; pH 7.4; 25°C) at a flow rate of 1 ml/min. Drugs were bath applied via the perfusion system. Perfusate (100 μl) was collected every 30 s before and following agonist stimulation and ATP levels were quantified using the luciferin-luciferase reagent (100 μl; Adenosine Triphosphate Assay Kit, Sigma). Bioluminescence was measured using a luminometer (TD-20/20, Turner Biosystems, Sunnyvale, CA) whose detection limit was ~5 fmol ATP/sample. Data were normalized by comparison to the peak ATP release induced by the calcium ionophore ionomycin (5 μM; Sigma) used as a control at the end of each experiment. In these experiments, oxotremorine sesquifumarate salt (OxoS) was used instead of OxoM because OxoM interfered with the assay. Pooled data are from a minimum of three cultures. Data analysis was performed using Excel (Microsoft) and Prism 4 (GraphPad Software, San Diego, CA).

Drugs and experimental protocols

Drugs used in this study (Table 2) were dissolved in external solution from concentrated stock solutions. The control vehicle (0.01% DMSO) used for dissolving 4-DAMP, AF-DX 116, U-73122, U-73343, and OAG did not produce an increase in $[Ca^{2+}]_i$. In experiments performed in the absence of external Ca^{2+}, Ca^{2+} was exchanged for equimolar concentration of magnesium and EGTA (2 mM) was added. In Ca^{2+} imaging experiments where concentration-dependent curves were constructed, two concentrations of OxoM, one low (0.001–5 μM) and one high (5–20 μM), were tested on each coverslip. In Ca^{2+} imaging and ATP release experiments where both agonists and antagonists were used, the order of drug application was the following: the agonist (30–90 s; i.e., OxoM, muscarine), followed by a washout (~10–20 min), preincubation with the antagonist (~10–20 min; i.e., AMN, PPADS), and another application of the agonist (30–90 s) in the presence of the antagonist.

Statistical analysis

Statistical significance was tested using paired *t*-test, unpaired *t*-test, and ANOVA followed by Bonferroni post hoc test (significance set at $P < 0.05$) using Prism 4 (GraphPad Software). Throughout the text, data are presented as means ± SE.

Results

Recordings presented in this study were made from rat urothelial cells that were in culture for 2 to 4 days. During the first and second day in culture, dissociated urothelial cells are initially present as single cells that start to divide and form small islands (Fig. 1, A–B and inset in B), similar to that described in previous studies (see Fig. 1 in Ref. 60). Over the course of several days urothelial cells continue to proliferate ultimately becoming confluent

(Fig. 1, C–I). In the time window of 2 to 4 days that we used these cultures, the majority of cells (90–95%) exhibited immunoreactivity for cytokeratin 17 (Fig. 1, J–K), a marker of basal/intermediate cell type (1, 45, 46, 51). Very few (<5%) cells exhibited immunoreactivity for cytokeratin 20, a marker of umbrella cell type (1, 45, 46, 51). As the efficiency of fura-2 loading was in general greater for cells forming small islands than for cells located in larger islands, cells localized in small islands were used for Ca^{2+} imaging experiments.

Expression of muscarinic urothelial receptors

RT-PCR detected the expression of all five mAChR subtypes M_1 to M_5 in cultured urothelial cells ($n = 4$ cultures; Fig. 2A). The level of expression was $M_2 > M_3 > M_5 > M_1 > M_4$. All mAChR subtypes were also present in native urothelial tissue (Fig. 2B; $n = 3$ experiments).

Using fura-2 calcium imaging and luciferin-luciferase for ATP detection, we next investigated whether mAChRs are functional and whether their activation might release factors that in vivo could potentially affect the afferent and/or the efferent nerves.

Activation of mAChRs increases $[Ca^{2+}]_i$ in cultured rat urothelial cells

Fura-2 calcium imaging showed that muscarinic agonists including ACh (10 μM), muscarine (1–20 μM), and OxoM (0.1–20 μM) increased $[Ca^{2+}]_i$ in cultured urothelial cells (Fig. 3). Generally, two to four reproducible responses could be elicited when stimulating the cells for 30–90 s every 5–15 min. Responses were greatly reduced or abolished by the muscarinic receptor antagonist atropine methyl nitrate (AMN; 10 μM; preincubation 10–15 min; Fig. 3). By itself, AMN (10 μM) increased baseline Ca^{2+} levels in 18% of cells (8/43; by 67.9 ± 11.3%, paired *t*-test, $P < 0.05$).

ACh (10 μM, 30- to 60-s application) increased $[Ca^{2+}]_i$ in 46% of cells (32/70) and responses were abolished or greatly reduced after the addition of AMN (10 μM; Fig. 3A). Because urothelial cells also express nicotinic receptors whose activation can increase $[Ca^{2+}]_i$ (2), specific agonists of muscarinic receptors, muscarine or OxoM, were used for the subsequent experiments. Muscarine (1–20 μM, 30- to 60-s application), a nonselective mAChR agonist, elicited transient Ca^{2+} responses in 21.5% of cells (19/88) that were abolished in the presence of AMN (10 μM; Fig. 3A). In four cells (21%), muscarine produced Ca^{2+} oscillations (0.66 ± 1.14 oscillations/min), suggesting Ca^{2+} release from internal stores (3).

OxoM (0.001–20 μM; 30- to 90-s application), another nonselective mAChR agonist, produced concentration-dependent increases in $[Ca^{2+}]_i$ in cultured urothelial cells (Fig. 3 and Table 3). Fitting of the data using a logistic function $y = A_2 + (A_1 - A_2)/1 + (x/x_0)^p$, as described in MATERIALS AND METHODS, yielded the following values for these parameters: A_1 was 9.88 ± 2.62, A_2 was 21.74 ± 1.48, P was 2.95 ± 4.32, and x_0 (EC_{50}) was 5.33 ± 2.31 E^{-8} M. OxoM triggered oscillations in 4% of cells (5/128; frequency 0.57 ± 0.03 oscillations/min).

Since activation of mAChRs leads to release of ATP (see next data set), we tested whether activation of purinergic receptors could contribute to OxoM-evoked $[Ca^{2+}]_i$ changes. The purinergic antagonist PPADS (20 μM), which blocks most of the P2X receptors and a few of P2Y receptors ($P2Y_1$, $P2Y_4$, $P2Y_6$) (39), had no effect on OxoM (20 μM)-evoked responses (Fig. 4, A and B, $n = 14$ cells; *t*-test, $P > 0.05$), while in the same cells it significantly reduced ATP (10 μM)-evoked responses (Fig. 4C, *t*-test, $P < 0.05$). In addition, OxoM responses differed from ATP responses in regard to the rise time (measured from baseline to peak response). Ca^{2+} responses triggered by OxoM (20 μM) had significantly slower rise

times than those triggered by ATP (10 μM; Fig. 4, D and E; 37.8 ± 1.7 s, n = 128 cells for OxoM responses compared with 18.5 ± 1.2 s, n = 65 for ATP responses; unpaired t-test, $P < 0.05$), suggesting that the pathways of $[Ca^{2+}]_i$ increases induced by the two stimuli may be different.

Sources of OxoM-evoked increases in $[Ca^{2+}]_i$

As mAChRs can trigger release of Ca^{2+} from the internal stores as well as influx of Ca^{2+} from the extracellular milieu in different cell types (11,29,37,40,43,44,48), we dissected the sources of $[Ca^{2+}]_i$ increases. Influx of Ca^{2+} from the extracellular milieu vs. release of Ca^{2+} from internal stores was tested by activating mAChRs in the presence and absence of extracellular calcium (Fig. 5). Removal of external Ca^{2+} abolished OxoM-elicited responses in 63% of cells (41/65; from 40.9 ± 8.2 to 2.2 ± 0.3% ΔR/R; paired t-test, $P < 0.05$; Fig. 5, A and C). In the remaining 37% of OxoM-responsive cells (24/65), Ca^{2+} responses were reduced by 56.9 ± 9.2% (n = 24; from 95.0 ± 10.2% to 46.0 ± 7.1% ΔR/R; paired t-test, $P < 0.05$; Fig. 5, B and D). The rise times for OxoM-evoked Ca^{2+} responses were not different between these two groups of cells (Fig. 5E; Gr 1: 35.3 ± 2.7 s, n = 41 cells compared with Gr 2: 31.4 ± 4.7 s, n = 24 cells; unpaired t-test, $P > 0.05$).

mAChR subtypes involved in increases in $[Ca^{2+}]_i$

Because the mRNA of M_1, M_2, and M_3 mAChR subtypes were expressed in urothelial cells at high levels, pharmacological agents (agonists and antagonists) were used to evaluate the contribution of these receptor subtypes to the intracellular Ca^{2+} changes. To assess the presence of M_1 mAChR subtype, we used the M_1-specific agonist McN-A-343 at a concentration of 10 μM, based on previous studies in bladder autonomic neurons (42). To assess the presence of M_2, M_3 mAChR subtypes, we used M_2- and M_3-specific antagonists, AF-DX 116 and 4-DAMP, respectively, both at a concentration of 10 μM. This concentration was chosen based on the fact that both antagonists are competitive and had to compete with 20 μM OxoM, a concentration that gave robust Ca^{2+} responses in a high percentage of cells.

Application of the M_1 mAChR agonist McN-A-343 (10 μM; Fig. 6A) increased $[Ca^{2+}]_i$ in 25.9% of cells (34/131) by 15.5 ± 1.4% above baseline (paired t-test, $P < 0.05$). Addition of AMN (5–10 μM; preincubation 10–15 min) abolished McN-A-343-elicited Ca^{2+} responses (n = 9 cells; Fig. 6A).

AF-DX 116 (10 μM; Fig. 6B), an M_2 mAChR antagonist, reduced the responses to OxoM (20 μM) in 94% of cells (31/33; from 10.4 ± 1.2 to 4.5 ± 1.1% ΔR/R; paired t-test, $P < 0.05$) and had no effect in the remaining 6% of cells (2/33). AF-DX 116 by itself did not increase $[Ca^{2+}]_i$.

4-DAMP (10 μM; Fig. 6C), an M_3 mAChR antagonist, reduced the responses to OxoM (20 μM) in 34% of cells (18/53; from 16.3 ± 5.7 to 6.1 ± 1.6% ΔR/R; paired t-test, $P < 0.05$; Fig. 6, Ci and Cii). Interestingly, 4-DAMP increased and/or unmasked the response to OxoM in 62% of cells (33/53, from 5.0 ± 0.6 to 27.4 ± 6.9% ΔR/R; paired t-test, $P < 0.05$; Fig. 6, Ciii and Civ). Upon washout of 4-DAMP, in most cells OxoM responses did not return to baseline and four cells (3 of the cells exhibiting a facilitated response and 1 whose response was inhibited by 4-DAMP) started to oscillate. 4-DAMP had no effect on 4% of cells (2/53) and by itself did not increase $[Ca^{2+}]_i$.

Intracellular pathways activated by mAChRs

M_1, M_3, and M_5 mAChR subtypes are able to activate the PLC-IP_3 pathway resulting in release of calcium from the intracellular stores (11). To test the involvement of this pathway

in OxoM-mediated $[Ca^{2+}]_i$ increases in urothelial cells, we used the PLC inhibitor U-73122 (2.5–5 μM) and its inactive analog U-73343 (2.5–5 μM) in the presence of the M_2 antagonist AF-DX 116 (1 μM). In 2 mM external Ca^{2+} concentration, the PLC inhibitor abolished OxoM-evoked Ca^{2+} responses in 68.2% (30/44) of cells, while in the remaining 14 cells OxoM triggered responses that did not return to baseline (Fig. 7A), indicative of cells no longer being able to handle an increase in the intracellular Ca^{2+}. In five of the above coverslips treated with U-73122, same cells or cells from different areas were tested after 30- to 50-min wash. Only 1 cell of 90 cells tested responded to OxoM, indicating that the effect of U-73122 was not reversible within this short period of time. The inactive analog U-73443 (2.5–5 μM) had no effect on OxoM-evoked responses (Fig. 7B).

The involvement of the PLC pathway was also tested in the absence of extracellular Ca^{2+} (Fig. 7C). Because multiple applications of OxoM in the absence of extracellular Ca^{2+} might deplete the internal stores, experiments were performed using coverslips that were incubated for 10–15 min in 0 mM external Ca^{2+} in the following three conditions: *1*) not treated (control), *2*) treated with the PLC inhibitor U-73122 (2.5 μM), or *3*) treated with the inactive analog U-73433 (2.5 μM). In these conditions, only 4% of cells (1/26) responded to OxoM in the coverslips treated with the PLC inhibitor while 47.7 and 53.4% of cells responded in the absence of PLC inhibitor or in the presence of the inactive analog U-73433 (2.5 μM), respectively (Fig. 7C). Together, these experiments suggest that activation of mAChRs (M_1, M_3, or M_5) can increase intracellular calcium via activation of the PLC pathway.

One possible way by which activation of mAChRs increases $[Ca^{2+}]_i$ independent of the intracellular stores might be via production of DAG and subsequent activation of TRP channels as shown in other cell types (49). To test the possibility that in cultured urothelial DAG activation increases $[Ca^{2+}]_i$, we used OAG (10 μM; 2-min application), a membrane-permeable analog of DAG. OAG increased $[Ca^{2+}]_i$ in 18.5% of cells (20/108; 8.25 ± 2.1% ΔR/R; 7 coverslips from 4 cultures), suggesting that if mAChRs are coupled to this pathway, this can result in $[Ca^{2+}]_i$ increases.

Activation of mAChRs releases ATP from rat urothelial cells

Muscarinic agonists including ACh (0.1–20 μM), muscarine (20 μM), and OxoS (20 μM) evoked ATP release from cultured urothelial cells (Fig. 8). In these experiments, OxoS was used instead of OxoM because OxoM interfered with the ATP assay.

ACh at 0.1 μM evoked consistent and repeatable ATP release that was not maximal relative to the calcium ionophore ionomycin (Fig. 8B). ACh (0.1 μM)-induced ATP release was reduced to 64.9 ± 18.7% of control by the M_2 mAChR antagonist AF-DX 116 (50 μM; paired *t*-test, $P > 0.05$), to 31.9 ± 10.4% of control by the M_3 mAChR antagonist 4-DAMP (50 μM; paired *t*-test, $P < 0.05$), and to 28.3 ± 16.2% of control by a combination of both antagonists (paired *t*-test, $P < 0.05$; Fig. 8C). These data indicated that even at high concentrations of antagonists, ACh was still able to release ATP, likely through activation of nAChRs present in urothelial cells (2). Thus, specific mAChR agonists and antagonists were used in subsequent experiments.

Muscarine (20 μM) evoked ATP release that was 9.54 ± 2.39% of the ionomycin response. Subsequent addition of AMN (20 μM) abolished this response (reduced by 98.78 ± 0.64%, paired *t*-test, $P < 0.05$; Fig. 8D). The M_1 mAChR agonist McN-A-343 (1 μM) evoked ATP release that was 8.08 ± 2.65% of ionomycin response (Fig. 8D). Two applications of OxoS (20 μM) at a 20-min interval evoked ATP release that lasted for 1 to 6 min and was 26.9 ± 14.6 and 18.6 ± 5.0% of ionomycin responses (Fig. 8E; 1st response: 44.13 ± 13.23 fmol ATP/100 μl, 2nd response: 41.44 ± 15.17 fmol ATP/100 μl and ionomycin response: 305.34 ± 135.28 fmol ATP/100 μl). OxoS responses were abolished by addition of AMN (20 μM;

reduced from 21.74 ± 2.1 to 1.18 ± 0.03% relative to the ionomycin response, paired *t*-test, $P < 0.05$; Fig. 8F). The M_2 mAChR antagonist AF-DX 116 (1 μM) reduced OxoS (20 μM)-evoked ATP responses by 46.06 ± 5.60% (paired *t*-test, $P < 0.05$; Fig. 8E). The M_3 mAChR antagonist 4-DAMP (1 μM) reduced OxoS (20 μM)-evoked ATP release by 84.7 ± 5.5% (paired *t*-test, $P < 0.05$; Fig. 8F). Taken together, these results indicated that activation of urothelial mAChRs caused ATP release and it is likely that M_1, M_2, and M_3 mAChR subtypes were involved.

Discussion

This study demonstrated that cultured urothelial cells from rat express functional mAChRs whose activation can alter $[Ca^{2+}]_i$ and trigger ATP release. RT-PCR identified mRNA of all five muscarinic receptor subtypes. Fura-2 Ca^{2+} imaging and the luciferin-luciferase assay showed that M_1, M_2, and M_3 mAChR subtypes were able to regulate $[Ca^{2+}]_i$ and to trigger release of ATP. Together with previous data suggesting a role of urothelial muscarinic receptors in vivo (30,52), these data suggest that several subtypes of urothelial mAChRs could contribute to the putative sensory functions of urothelial cells.

Urothelial cells express functional mAChRs whose activation increases $[Ca^{2+}]_i$

Recent investigations showed that the urothelium of different species, including humans, expresses mRNA or protein of M_1 to M_5 mAChR subtypes (10,13,21,22,28,33,34,59). Immunostaining in tissue from mouse and human showed that different mAChR subtypes are expressed in different layers of the urothelium. M_1 mAChRs seemed to be expressed in the basal cells, M_2 mAChRs appeared restricted to the umbrella cells while M_3, M_4, M_5 mAChRs were found throughout the urothelium (10,59). Our cultured rat urothelial cells were mostly positive for cytokeratin 17 (Fig. 1), a marker for basal/intermediate cells, with very few cells positive for cytokeratin 20, a marker for umbrella cells (1,45,46,51), in the time window that we studied these cells (2–4 days). RT-PCR from these cultures and also from native urothelial tissue confirmed the expression of all five subtypes of mAChRs (Fig. 2).

Using several methods we showed that activation of M_1, M_2, and M_3 mAChR subtypes can alter $[Ca^{2+}]_i$ and can release ATP in cultured rat urothelial cells (Figs. 3–8). Fura-2 Ca^{2+} imaging data indicated that activation of urothelial mAChRs increases $[Ca^{2+}]_i$ in ~50% of the cells (Fig. 3). The reason for lack of responses in ~50% of cells is uncertain. It seems likely that muscarinic agonist-induced Ca^{2+} responses were directly related to mAChR activation rather than to activation of purinergic receptors by OxoM-evoked ATP release, because PPADS (20 μM), a purinergic receptor antagonist that blocks primarily P2X receptors and a few P2Y receptors ($P2Y_1$, $P2Y_4$, $P2Y_6$) (39), had no effect on OxoM-evoked Ca^{2+} responses while it significantly reduced ATP-evoked Ca^{2+} response (Fig. 4, A, B, C). In addition, because we used a perfused preparation (flow rate 1.5–2 ml/min), the ATP released from a cell would probably be washed away before accumulating to give rise to a Ca^{2+} response. Furthermore, the rise time of OxoM-evoked Ca^{2+} responses was significantly longer than the rise time of ATP-evoked Ca^{2+} responses (Fig. 4, D, E), consistent with the fact that mAChRs increase $[Ca^{2+}]_i$ by activating second messenger pathways (11), whereas ATP increases $[Ca^{2+}]_i$ most likely via ligand-gated ion channels (P2X) (39).

The potency of OxoM in cultured urothelial cells appeared to be similar to what has been reported in rat bladder smooth muscle (50) or in rat cortical neurons (36). In rat bladder smooth muscle preparation, OxoM was more potent than ACh or bethanechol at inducing smooth muscle contraction (pD2 values were 6.38 ± 0.25, 4.82 ± 0.24, and 4.42 ± 0.14 for OxoM ACh and bethanechol, respectively) (50).

Several studies performed in cell types from different species including epithelial cells from chick embryo lens (37), endothelial cells from mouse aorta (48), smooth muscle of swine trachea (43), human colon (29), or human esophagus (44) showed that ACh can increase $[Ca^{2+}]_i$ by activating mAChRs that trigger downstream mechanisms involving influx of calcium from the extracellular milieu and release from intracellular stores. When we dissected the sources of $[Ca^{2+}]_i$ increases, cells fell into two groups (Fig. 5). In one group, representing 63% of the cells, extracellular Ca^{2+} influx was the main source of increases in $[Ca^{2+}]_i$, whereas in the second group both external and internal Ca^{2+} sources were important. In this later group, activation of the PLC-IP_3 pathway is a possible mechanism for mAChR-mediated changes in $[Ca^{2+}]_i$ (Fig. 7). Depletion of those stores could, in turn, trigger Ca^{2+} influx through Ca^{2+}-permeable channels (CRAC channels). Candidates for such channels are the transient receptor potential (TRP) channels that are Ca^{2+}-permeable cation channels that can be activated by stimulation of G_q-coupled receptors (54) and thus could potentially be activated by M_1, M_3, or M_5 mAChR subtypes. Urothelial cells express TRP channels of the vanilloid and melastatin families (TRPV and TRPM channels) which are involved in detection of temperature and osmolarity [TRPV1 (9); TRPV4 (4); TRPM8 (5,8,47)]. In the larger group of urothelial cells, influx from the extracellular milieu was the major source of $[Ca^{2+}]_i$ changes. A similar dependence of $[Ca^{2+}]_i$ increases on extracellular Ca^{2+} influx has been shown in cultured DRG neurons, most likely due to M_3 mAChR subtype activation (24). How can mAChRs trigger Ca^{2+} influx without the involvement of the internal stores? One possibility is mAChR-induced stimulation of diglycerol (DAG) production which, in turn, can activate Ca^{2+}-permeable TRP channels (49,53). This is consistent with our data indicating that OAG, a synthetic membrane-permeable analog of DAG, can also increase $[Ca^{2+}]_i$ in cultured urothelial cells.

mAChR subtypes involved in $[Ca^{2+}]_i$ changes

We attempted to distinguish pharmacologically which mAChR subtypes are involved in $[Ca^{2+}]_i$ changes. Due to limitations in the availability of agonists and antagonists selective for different mAChR subtypes, we used the M_1 mAChR agonist McN-A-343 and the M_2 and M_3 mAChR antagonists, AF-DX 116 and 4-DAMP, respectively (Fig. 6). These drugs have been shown to exhibit selectivity for M_1, M_2, M_3 mAChR subtypes, respectively, although minimal effects on other subtypes have been reported. In expression systems, 4-DAMP displayed some affinity for M_5 subtype (56) and also for M_2 subtype in bladder smooth muscle (33). AF-DX 116 also might have some effects on M_3 subtype in the bladder depending on the concentrations (33). The concentrations used in this study (10 μM) that were rather on the high side were chosen to compete with a high concentration of OxoM (20 μM; which produced consistent and robust Ca^{2+} imaging responses in a large number of cells), therefore some nonselective receptor blockade might have occurred. Our results suggest that M_1 mAChR subtype mediated $[Ca^{2+}]_i$ changes in 27% of the cells and M_2, M_3 mAChR subtypes mediated $[Ca^{2+}]_i$ changes in 93% of OxoM-responsive cells (which represent ~50% of total urothelial cells; Fig. 6). Results from binding studies in human bladder mucosa indicate that the main receptor subtype is M_2, representing ~70% of the total number of mAChRs, whereas M_1 represents ~7% and M_3/M_5 ~25% (33).

Because M3- as well as M_1-elicited Ca^{2+} responses seem to involve the PLC-IP_3 signaling pathway followed by release of Ca^{2+} from the internal stores (Fig. 7) (11), it was anticipated that blocking M_3 mAChR would reduce or eliminate Ca^{2+} responses. This did occur in a subpopulation of cells (~34%) where the M_3 antagonist 4-DAMP eliminated or reduced the OxoM-elicited Ca^{2+} responses. However, in a larger subpopulation of cells (~62%) 4-DAMP facilitated or unmasked Ca^{2+} responses (Fig. 6). These results suggest interaction(s) between the M_3 mAChR subtype and other mAChR subtypes that alter $[Ca^{2+}]_i$ in urothelial cells. The mechanisms for facilitation and possible interactions among mAChR subtypes

remain to be investigated. The participation of M_2 mAChRs in OxoM-elicited Ca^{2+} response was unexpected as activation of M_2 mAChR inhibits adenylate cyclase activity rather than increasing IP_3 (11). However, a similar contribution of the M_2 receptor subtype to muscarinic-mediated $[Ca^{2+}]_i$ changes was reported in porcine airway smooth muscle cells (57) and in duodenal myocytes (19), where M_2 was shown to mediate ryanodine receptor-dependent $[Ca^{2+}]_i$ oscillations (19). Oscillations were also seen in our study in response to muscarine (in ~20% of cells) and to OxoM (in ~4% of cells), suggesting that a similar pathway might be playing a role in urothelial cells. The high density of the M_2 receptor subtype in the urothelium (>70%) (33), coupled with results from this study indicating that M_2 can regulate $[Ca^{2+}]_i$ levels, raises the possibility that urothelial M_2 mAChR subtypes might play a significant physiological role in bladder functions.

mAChR activation causes ATP release

mAChR-mediated increases in $[Ca^{2+}]_i$ can serve various functions including ATP release. Previous studies showed that in cat cultured urothelial cells hypotonic solution-induced ATP release is Ca^{2+} dependent and depends on both Ca^{2+} influx from the extracellular milieu and Ca^{2+} release from IP_3-sensitive intracellular stores (7). In the present study, we found that activation of mAChRs caused ATP release and that M_1, M_2, M_3 receptor subtypes were involved (Fig. 8). It has been well-established that ATP is released from the urothelium in response to bladder stretch (in rabbit, pig, and human) (17,31) and that ATP acting on purinergic receptors ($P2X_3$) located on the afferent sensory nerves (14,32,55) can initiate bladder reflexes and possibly bladder pain (17,35). Recent data from in vivo CMG studies also suggest that activation of mAChRs located on the bladder sensory pathways (urothelium and/or sensory nerves) has an excitatory effect on the micturition reflex, which is reduced by blocking purinergic receptors (30).

Conclusions

In summary, the distribution of mAChR subtypes in distinct urothelial and suburothelial layers (10,59) coupled with their ability to activate specific mechanisms for altering $[Ca^{2+}]_i$ levels (Figs. 5 and 6), and to release ATP (Fig. 8) that can influence bladder function (17,35) by acting on urothelial and suburothelial afferent nerves, suggest a significant role of urothelial mAChRs in bladder sensation and function. A further analysis of the subtypes of urothelial mAChRs, their intracellular signaling mechanisms, and their role in bladder function in vivo in normal and pathological conditions could be beneficial for the identification of new drug targets for treatment of overactive bladder.

Acknowledgments

The authors thank S. Zilavy for editorial help and members of W. C. de Groat and L. A. Birder laboratories for valuable discussions.

Grants: This work was supported by a grant from the American Foundation for Urologic Disease/American Urological Association Research Scholar Program to F. A. Kullmann (Negoita), National Institute of Diabetes and Digestive and Kidney Diseases (NIDDK) Grant 49430 to W. C. de Groat, and NIDDK Grant 54824 to L. A. Birder.

References

1. Apodaca G. The uroepithelium: not just a passive barrier. Traffic. 2004; 5:117–128. [PubMed: 15086788]
2. Beckel JM, Kanai A, Lee SJ, de Groat WC, Birder LA. Expression of functional nicotinic acetylcholine receptors in rat urinary bladder epithelial cells. Am J Physiol Renal Physiol. 2006; 290:F103–F110. [PubMed: 16144967]

3. Berridge MJ. Calcium microdomains: organization and function. Cell Calcium. 2006; 40:405–412. [PubMed: 17030366]
4. Birder L, Kullmann FA, Lee H, Barrick S, de Groat W, Kanai A, Caterina M. Activation of urothelial transient receptor potential vanilloid 4 by 4alpha-phorbol 12,13-didecanoate contributes to altered bladder reflexes in the rat. J Pharmacol Exp Ther. 2007; 323:227–235. [PubMed: 17636010]
5. Birder LA. More than just a barrier: urothelium as a drug target for urinary bladder pain. Am J Physiol Renal Physiol. 2005; 289:F489–F495. [PubMed: 16093424]
6. Birder LA, Apodaca G, de Groat WC, Kanai AJ. Adrenergic- and capsaicin-evoked nitric oxide release from urothelium and afferent nerves in urinary bladder. Am J Physiol Renal Physiol. 1998; 275:F226–F229.
7. Birder LA, Barrick SR, Roppolo JR, Kanai AJ, de Groat WC, Kiss S, Buffington CA. Feline interstitial cystitis results in mechanical hypersensitivity and altered ATP release from bladder urothelium. Am J Physiol Renal Physiol. 2003; 285:F423–F429. [PubMed: 12759226]
8. Birder LA, de Groat WC. Mechanisms of disease: involvement of the urothelium in bladder dysfunction. Nat Clin Pract Urol. 2007; 4:46–54. [PubMed: 17211425]
9. Birder LA, Nakamura Y, Kiss S, Nealen ML, Barrick S, Kanai AJ, Wang E, Ruiz G, De Groat WC, Apodaca G, Watkins S, Caterina MJ. Altered urinary bladder function in mice lacking the vanilloid receptor TRPV1. Nat Neurosci. 2002; 5:856–860. [PubMed: 12161756]
10. Bschleipfer T, Schukowski K, Weidner W, Grando SA, Schwantes U, Kummer W, Lips KS. Expression and distribution of cholinergic receptors in the human urothelium. Life Sci. 2007; 80:2303–2307. [PubMed: 17335853]
11. Caulfield MP. Muscarinic receptors–characterization, coupling and function. Pharmacol Ther. 1993; 58:319–379. [PubMed: 7504306]
12. Chaiyaprasithi B, Mang CF, Kilbinger H, Hohenfellner M. Inhibition of human detrusor contraction by a urothelium derived factor. J Urol. 2003; 170:1897–1900. [PubMed: 14532802]
13. Chess-Williams R. Muscarinic receptors of the urinary bladder: detrusor, urothelial and prejunctional. Auton Autacoid Pharmacol. 2002; 22:133–145. [PubMed: 12452898]
14. Cockayne DA, Hamilton SG, Zhu QM, Dunn PM, Zhong Y, Novakovic S, Malmberg AB, Cain G, Berson A, Kassotakis L, Hedley L, Lachnit WG, Burnstock G, McMahon SB, Ford AP. Urinary bladder hyporeflexia and reduced pain-related behaviour in P2X3-deficient mice. Nature. 2000; 407:1011–1015. [PubMed: 11069181]
15. de Groat WC. Integrative control of the lower urinary tract: preclinical perspective. Br J Pharmacol. 2006; 147 2:S25–S40. [PubMed: 16465182]
16. Ene FA, Kullmann PH, Gillespie DC, Kandler K. Glutamatergic calcium responses in the developing lateral superior olive: receptor types and their specific activation by synaptic activity patterns. J Neurophysiol. 2003; 90:2581–2591. [PubMed: 12853437]
17. Ferguson DR, Kennedy I, Burton TJ. ATP is released from rabbit urinary bladder epithelial cells by hydrostatic pressure changes–a possible sensory mechanism? J Physiol. 1997; 505:503–511. [PubMed: 9423189]
18. Finney SM, Andersson KE, Gillespie JI, Stewart LH. Antimuscarinic drugs in detrusor overactivity and the overactive bladder syndrome: motor or sensory actions? BJU Int. 2006; 98:503–507. [PubMed: 16925744]
19. Fritz N, Macrez N, Mironneau J, Jeyakumar LH, Fleischer S, Morel JL. Ryanodine receptor subtype 2 encodes Ca^{2+} oscillations activated by acetylcholine via the M_2 muscarinic receptor/cADP-ribose signalling pathway in duodenum myocytes. J Cell Sci. 2005; 118:2261–2270. [PubMed: 15870112]
20. Gabella G, Davis C. Distribution of afferent axons in the bladder of rats. J Neurocytol. 1998; 27:141–155. [PubMed: 10640174]
21. Giglio D, Andersson M, Aronsson P, Delbro DS, Haraldsson B, Tobin G. Changes in muscarinic receptors in the toad urothelial cell line TBM-54 following acrolein treatment. Clin Exp Pharmacol Physiol. 2008; 35:217–222. [PubMed: 17941892]

22. Giglio D, Ryberg AT, To K, Delbro DS, Tobin G. Altered muscarinic receptor subtype expression and functional responses in cyclophosphamide induced cystitis in rats. Auton Neurosci. 2005; 122:9–20. [PubMed: 16125470]
23. Gillespie JI, Markerink-van Ittersum M, de Vente J. Sensory collaterals, intramural ganglia and motor nerves in the guinea-pig bladder: evidence for intramural neural circuits. Cell Tissue Res. 2006; 325:33–45. [PubMed: 16525831]
24. Haberberger R, Scholz R, Kummer W, Kress M. M2-receptor subtype does not mediate muscarine-induced increases in $[Ca^{2+}]_i$ in nociceptive neurons of rat dorsal root ganglia. J Neurophysiol. 2000; 84:1934–1941. [PubMed: 11024086]
25. Hanna-Mitchell AT, Beckel JM, Barbadora S, Kanai AJ, de Groat WC, Birder LA. Non-neuronal acetylcholine and urinary bladder urothelium. Life Sci. 2007; 80:2298–2302. [PubMed: 17363007]
26. Hawthorn MH, Chapple CR, Cock M, Chess-Williams R. Urothelium-derived inhibitory factor(s) influences on detrusor muscle contractility in vitro. Br J Pharmacol. 2000; 129:416–419. [PubMed: 10711338]
27. Kanai A, Roppolo J, Ikeda Y, Zabbarova I, Tai C, Birder L, Griffiths D, de Groat W, Fry C. Origin of spontaneous activity in neonatal and adult rat bladders and its enhancement by stretch and muscarinic agonists. Am J Physiol Renal Physiol. 2007; 292:F1065–F1072. [PubMed: 17107944]
28. Kim JC, Yoo JS, Park EY, Hong SH, Seo SI, Hwang TK. Muscarinic and purinergic receptor expression in the urothelium of rats with detrusor overactivity induced by bladder outlet obstruction. BJU Int. 2008; 101:371–375. [PubMed: 17922866]
29. Kovac JR, Chrones T, Sims SM. Temporal and spatial dynamics underlying capacitative calcium entry in human colonic smooth muscle. Am J Physiol Gastrointest Liver Physiol. 2008; 294:G88–G98. [PubMed: 17975132]
30. Kullmann FA, Artim DE, Birder LA, de Groat WC. Activation of muscarinic receptors in rat bladder sensory pathways alters reflex bladder activity. J Neurosci. 2008; 28:1977–1987. [PubMed: 18287514]
31. Kumar V, Chapple CC, Chess-Williams R. Characteristics of adenosine triphosphate release from porcine and human normal bladder. J Urol. 2004; 172:744–747. [PubMed: 15247774]
32. Lee HY, Bardini M, Burnstock G. Distribution of P2X receptors in the urinary bladder and the ureter of the rat. J Urol. 2000; 163:2002–2007. [PubMed: 10799247]
33. Mansfield KJ, Liu L, Mitchelson FJ, Moore KH, Millard RJ, Burcher E. Muscarinic receptor subtypes in human bladder detrusor and mucosa, studied by radioligand binding and quantitative competitive RT-PCR: changes in ageing. Br J Pharmacol. 2005; 144:1089–1099. [PubMed: 15723094]
34. Mukerji G, Yiangou Y, Grogono J, Underwood J, Agarwal SK, Khullar V, Anand P. Localization of M2 and M3 muscarinic receptors in human bladder disorders and their clinical correlations. J Urol. 2006; 176:367–373. [PubMed: 16753445]
35. Namasivayam S, Eardley I, Morrison JF. Purinergic sensory neurotransmission in the urinary bladder: an in vitro study in the rat. BJU Int. 1999; 84:854–860. [PubMed: 10532986]
36. Nishikawa M, Munakata M, Akaike N. Muscarinic acetylcholine response in pyramidal neurones of rat cerebral cortex. Br J Pharmacol. 1994; 112:1160–1166. [PubMed: 7952877]
37. Oppitz M, Mack A, Drews U. Ca^{2+} mobilization and cell contraction after muscarinic cholinergic stimulation of the chick embryo lens. Invest Ophthalmol Vis Sci. 2003; 44:4813–4819. [PubMed: 14578403]
38. Pfaffl MW. A new mathematical model for relative quantification in real-time RT-PCR. Nucleic Acids Res. 2001; 29:e45. [PubMed: 11328886]
39. Ralevic V, Burnstock G. Receptors for purines and pyrimidines. Pharmacol Rev. 1998; 50:413–492. [PubMed: 9755289]
40. Sah P, Faber ES. Channels underlying neuronal calcium-activated potassium currents. Prog Neurobiol. 2002; 66:345–353. [PubMed: 12015199]
41. Scheenen WJ, Makings LR, Gross LR, Pozzan T, Tsien RY. Photodegradation of indo-1 and its effect on apparent Ca^{2+} concentrations. Chem Biol. 1996; 3:765–774. [PubMed: 8939693]

42. Sculptoreanu A, Yoshimura N, de Groat WC, Somogyi GT. Protein kinase C is involved in M1-muscarinic receptor-mediated facilitation of L-type Ca^{2+} channels in neurons of the major pelvic ganglion of the adult male rat. Neurochem Res. 2001; 26:933–942. [PubMed: 11699945]
43. Shieh CC, Petrini MF, Dwyer TM, Farley JM. Calcium mobilization and muscle contraction induced by acetylcholine in swine trachealis. J Biomed Sci. 1995; 2:272–282. [PubMed: 11725064]
44. Sims SM, Jiao Y, Preiksaitis HG. Regulation of intracellular calcium in human esophageal smooth muscles. Am J Physiol Cell Physiol. 1997; 273:C1679–C1689.
45. Southgate J, Harnden P, Trejdosiewicz LK. Cytokeratin expression patterns in normal and malignant urothelium: a review of the biological and diagnostic implications. Histol Histopathol. 1999; 14:657–664. [PubMed: 10212826]
46. Southgate J, Hutton KA, Thomas DF, Trejdosiewicz LK. Normal human urothelial cells in vitro: proliferation and induction of stratification. Lab Invest. 1994; 71:583–594. [PubMed: 7967513]
47. Stein RJ, Santos S, Nagatomi J, Hayashi Y, Minnery BS, Xavier M, Patel AS, Nelson JB, Futrell WJ, Yoshimura N, Chancellor MB, De Miguel F. Cool (TRPM8) and hot (TRPV1) receptors in the bladder and male genital tract. J Urol. 2004; 172:1175–1178. [PubMed: 15311065]
48. Suh SH, Vennekens R, Manolopoulos VG, Freichel M, Schweig U, Prenen J, Flockerzi V, Droogmans G, Nilius B. Characterisation of explanted endothelial cells from mouse aorta: electrophysiology and Ca^{2+} signalling. Pflügers Arch. 1999; 438:612–620.
49. Sydorenko V, Shuba Y, Thebault S, Roudbaraki M, Lepage G, Prevarskaya N, Skryma R. Receptor-coupled, DAG-gated Ca^{2+}-permeable cationic channels in LNCaP human prostate cancer epithelial cells. J Physiol. 2003; 548:823–836. [PubMed: 12724346]
50. Tong YC, Hung YC, Lin SN, Cheng JT. Pharmacological characterization of the muscarinic receptor subtypes responsible for the contractile response in the rat urinary bladder. J Auton Pharmacol. 1997; 17:21–25. [PubMed: 9201556]
51. Truschel ST, Ruiz WG, Shulman T, Pilewski J, Sun TT, Zeidel ML, Apodaca G. Primary uroepithelial cultures. A model system to analyze umbrella cell barrier function. J Biol Chem. 1999; 274:15020–15029. [PubMed: 10329705]
52. Ungerer, TD.; Roppolo, JR.; Tai, C.; De Groat, WC. Influence of urothelial and suburothelial muscarinic receptors on voiding in the spinal cord injured cat. Program No. 104.7; Society for Neuroscience Meeting; Washington, DC. 2005.
53. Venkatachalam K, Ma HT, Ford DL, Gill DL. Expression of functional receptor-coupled TRPC3 channels in DT40 triple receptor InsP3 knockout cells. J Biol Chem. 2001; 276:33980–33985. [PubMed: 11466302]
54. Venkatachalam K, Montell C. TRP channels. Annu Rev Biochem. 2007; 76:387–417. [PubMed: 17579562]
55. Vlaskovska M, Kasakov L, Rong W, Bodin P, Bardini M, Cockayne DA, Ford AP, Burnstock G. P2X3 knock-out mice reveal a major sensory role for urothelially released ATP. J Neurosci. 2001; 21:5670–5677. [PubMed: 11466438]
56. Watson N, Daniels DV, Ford AP, Eglen RM, Hegde SS. Comparative pharmacology of recombinant human M3 and M5 muscarinic receptors expressed in CHO-K1 cells. Br J Pharmacol. 1999; 127:590–596. [PubMed: 10385263]
57. White TA, Kannan MS, Walseth TF. Intracellular calcium signaling through the cADPR pathway is agonist specific in porcine airway smooth muscle. FASEB J. 2003; 17:482–484. [PubMed: 12551848]
58. Yoshida M, Miyamae K, Iwashita H, Otani M, Inadome A. Management of detrusor dysfunction in the elderly: changes in acetylcholine and adenosine triphosphate release during aging. Urology. 2004; 63:17–23. [PubMed: 15013648]
59. Zarghooni S, Wunsch J, Bodenbenner M, Bruggmann D, Grando SA, Schwantes U, Wess J, Kummer W, Lips KS. Expression of muscarinic and nicotinic acetylcholine receptors in the mouse urothelium. Life Sci. 2007; 80:2308–2313. [PubMed: 17337281]
60. Zhang YY, Ludwikowski B, Hurst R, Frey P. Expansion and long-term culture of differentiated normal rat urothelial cells in vitro. In Vitro Cell Dev Biol Anim. 2001; 37:419–429. [PubMed: 11573816]

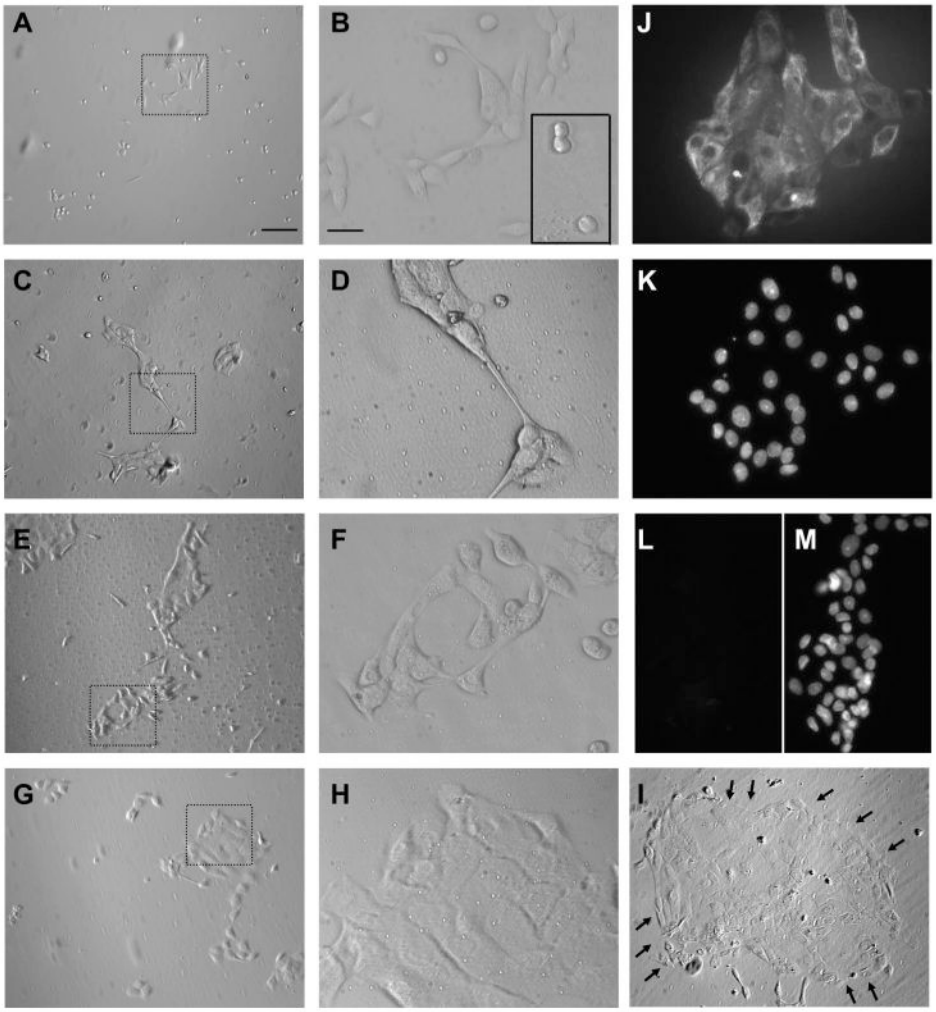

Fig. 1.

Micrographs of urothelial cells cultured for different periods of time (2–6 days). *A*–*I*: pictures of live urothelial cells that have been in culture for 2 (*A*, *B*), 3 (*C*, *D*), 4 (*E*, *F*), 5 (*G*, *H*), and 6 (*I*) days. *A*, *C*, *E*, *G*, and *I* are at ×10 magnification. Dotted areas in *A*, *C*, *E*, and *G* are shown in higher magnification (×40) in *B*, *D*, *F*, and *H*. *I*: arrows outline a large island of cells. *J*, *K*: pictures of the same field of cells stained with cytokeratin 17 (CK 17) antibodies (*J*) and with DAPI for nuclear staining (*K*), from a 2-day-old culture, indicating that the majority of cells were positive for CK 17. *L*, *M*: pictures of the same field of cells stained with cytokeratin 20 (CK 20) antibodies (*L*) and with DAPI for nuclear staining (*M*), from a 2-day-old culture, illustrating the absence of CK 20 in these cells. Cell density for culture shown in *A*–*I* was 60×10^4 cells/ml and for culture shown in *K*–*M* was 80×10^4 cells/ml. Scale bar for *A*, *C*, *E*, *G*, and *I* is 100 μm and is shown in *A*. Scale bar for *B*, *D*, *F*, *H*, and *J*–*M* is 25 μm and is shown in *B*.

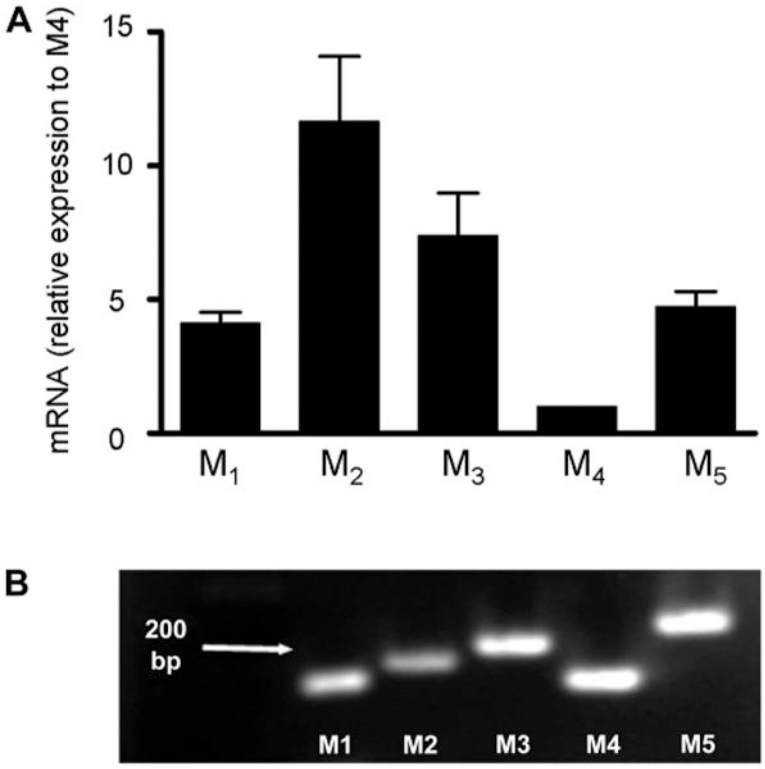

Fig. 2.

mRNA of all muscarinic acetylcholine receptor (mAChR) subtypes is expressed in rat cultured urothelial cells and urothelial tissue. *A*: RT-PCR data from cultured urothelial cells illustrating mRNA expression of M_1, M_2, M_3, and M_5 mAChR subtypes relative to the expression of M_4 mAChR subtype which was set to 1 (n = 4 experiments). *B*: agarose gel containing the products of RT-PCR from urothelial tissue, indicating the expression of all mAChR subtypes (n = 3 experiments).

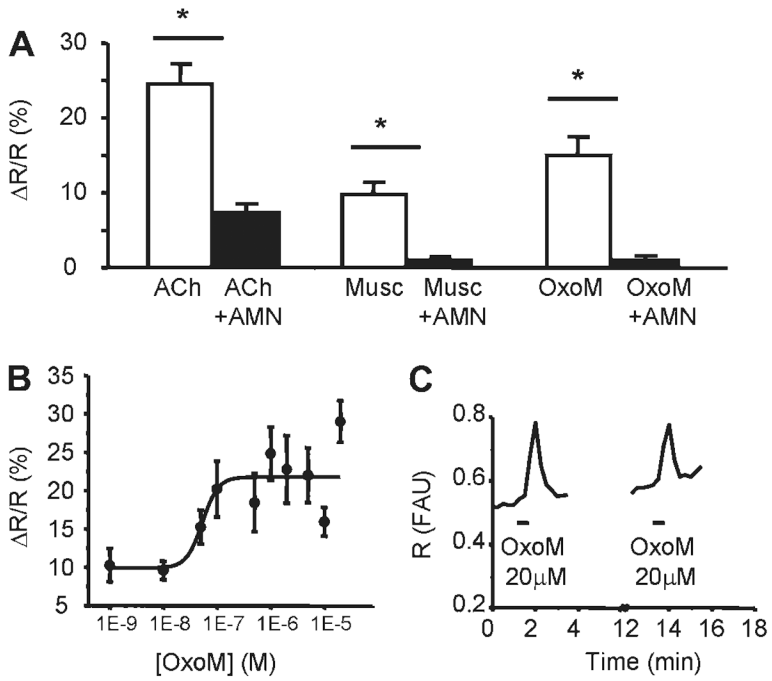

Fig. 3.

mAChR activation increases $[Ca^{2+}]_i$. *A*: muscarinic agonists ACh (10 μM, *n* = 22 cells), muscarine (10 μM, *n* = 11 cells), and oxotremorine methiodide (OxoM; 20 μM, *n* = 43 cells) increase intracellular calcium concentration. Responses are reduced or blocked by incubation with the muscarinic antagonist atropine methyl nitrate (AMN; 10 μM). *Significant differences ($P < 0.05$) tested with paired *t*-test. Data were collected from 3–12 coverslips from 3–5 cultures. *B*: concentration-response curve of OxoM-elicited $[Ca^{2+}]_i$ changes. Data were fitted with a logistic curve described by the equation $y = A_2 + (A_1 - A_2)/[1 + (x/x0)\hat{}p]$ (see MATERIALS AND METHODS). A_1 was 9.88 ± 2.62, A_2 was 21.74 ± 1.48, X_0 or EC_{50} was 5.33 ± 2.31E^{-8}, and P was 2.95 ± 4.32. Data were collected from 4–12 coverslips from 3–5 cultures (Table 3). *C*: example from a single urothelial cell of $[Ca^{2+}]_i$ increases evoked by repetitive applications of OxoM (20 μM). R = F_{340nm}/F_{380nm} which is proportional to the intracellular calcium concentration.

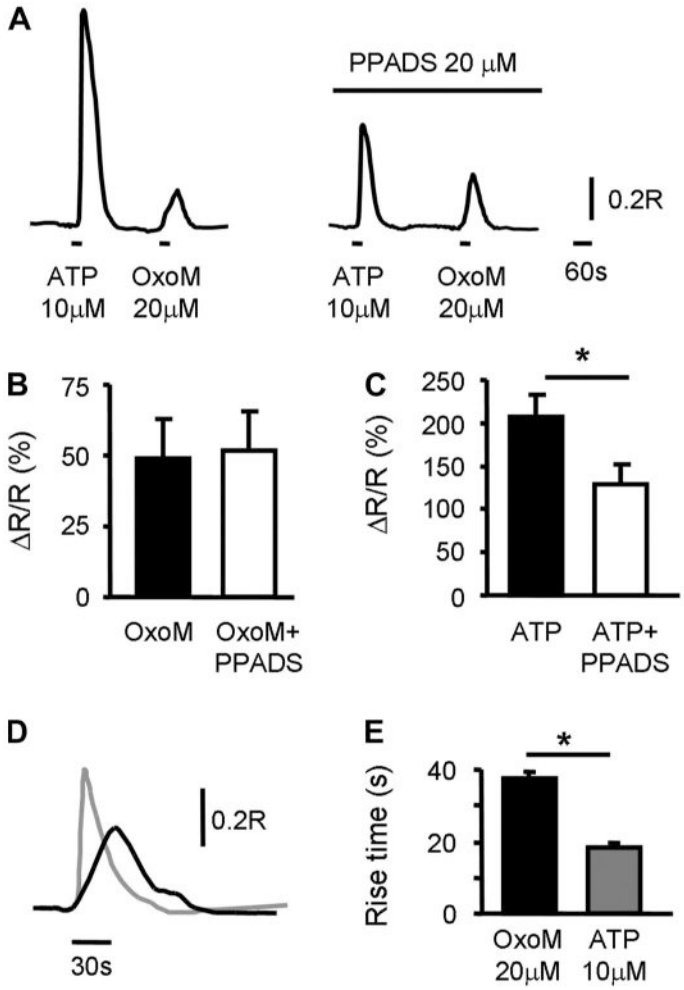

Fig. 4.

Role of purinergic receptors in OxoM-evoked Ca^{2+} responses. *A*: example of ATP (10 μM, 30-s application)- and OxoM (20 μM, 30-s application)-evoked Ca^{2+} responses in the absence and in the presence of PPADS (20 μM). Cells were preincubated with PPADS for 10–15 min. *B*, *C*: summary of OxoM-evoked Ca^{2+} responses (*B*) and ATP-evoked Ca^{2+} responses (*C*) from $n = 14$ cells. *Significant changes ($P < 0.05$) from control tested with paired *t*-test. *D*: rise times of OxoM- and ATP-evoked Ca^{2+} responses are different. Example of OxoM (20 μM, 30-s application; black trace) and ATP (10 μM, 30-s application; gray trace) responses from the same cell. Traces are superimposed and aligned with respect to the starting point of the Ca^{2+} response. *E*: summary of rise times. Data are from $n = 128$ cells for OxoM and $n = 65$ cells for ATP response. *Significant differences ($P < 0.05$) tested with unpaired *t*-test.

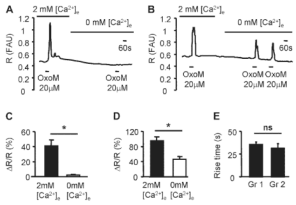

Fig. 5.

mAChR-mediated changes in $[Ca^{2+}]_i$ involve Ca^{2+} release from internal stores as well as Ca^{2+} influx from extracellular milieu. *A*: example from a single urothelial cell of an OxoM (20 μM, 60-s application)-elicited response in 2 mM external Ca^{2+} which was abolished when the external Ca^{2+} was removed. *B*: example from a single urothelial cell of an OxoM (20 μM, 60-s application)-elicited response in 2 mM external Ca^{2+} which was reduced when external Ca^{2+} was removed. *C*: summary from all cells in which the responses were abolished, termed *group 1* (*Gr 1*; *n* = 41 cells; 4 coverslips from 3 cultures). *D*: summary from all cells in which the responses were diminished but not abolished, termed *group 2* (*Gr 2*; *n* = 24 cells; 4 coverslips from 3 cultures). *C* and *D*: *Significant differences ($P < 0.05$) tested with paired *t*-test. *E*: summary of rise times from cells whose responses were abolished in 0 Ca^{2+} (*Gr 1*; *n* = 41 cells) and from cells whose responses were diminished (*Gr 2*; *n* = 24 cells). ns, No significant changes ($P > 0.05$) using unpaired *t*-test.

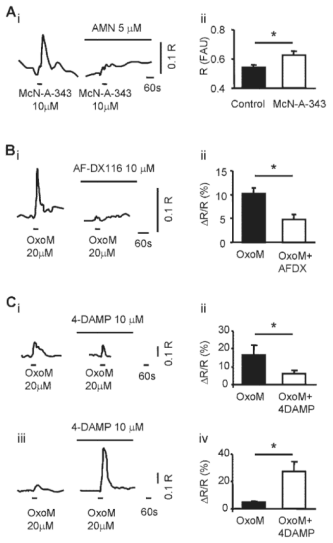

Fig. 6.

mAChR subtypes involved in $[Ca^{2+}]_i$ changes. *Ai*: example from a single urothelial cell of changes in $[Ca^{2+}]_i$ evoked by the M_1 mAChR agonist McN-A-343 (10 μM) and abolished by AMN (5 μM, *n* = 9 cells; 3 coverslips from 3 cultures). *Aii*: average fluorescence signal measured at the baseline before drug application (filled bar) and at the peak response to McN-A-343 (10 μM; open bar). Summary from *n* = 34 cells (5 coverslips from 3 cultures). *Bi*: example from a single urothelial cell of changes in $[Ca^{2+}]_i$ evoked by OxoM (20 μM) in the absence (*left* trace) and in the presence of the M_2 mAChR antagonist AF-DX116 (10 μM; *right* trace). *Bii*: summary from *n* = 31 cells (3 coverslips from 3 cultures). *Ci*: example from a single urothelial cell of changes in $[Ca^{2+}]_i$ evoked by OxoM (20 μM; *left* trace) and reduced by the M_3 mAChR antagonist 4-DAMP (10 μM; *right* trace). *Cii*: summary from *n* = 18 cells (3 coverslips from 3 cultures). *Ciii*: example from a single urothelial cell of changes in $[Ca^{2+}]_i$ evoked by OxoM (20 μM; *left* trace) and potentiated by the M_3 mAChR antagonist 4-DAMP (10 μM; *right* trace). *Civ*: summary from *n* = 33 cells (3 coverslips from 3 cultures). *Statistically significant differences ($P < 0.05$) using paired *t*-test.

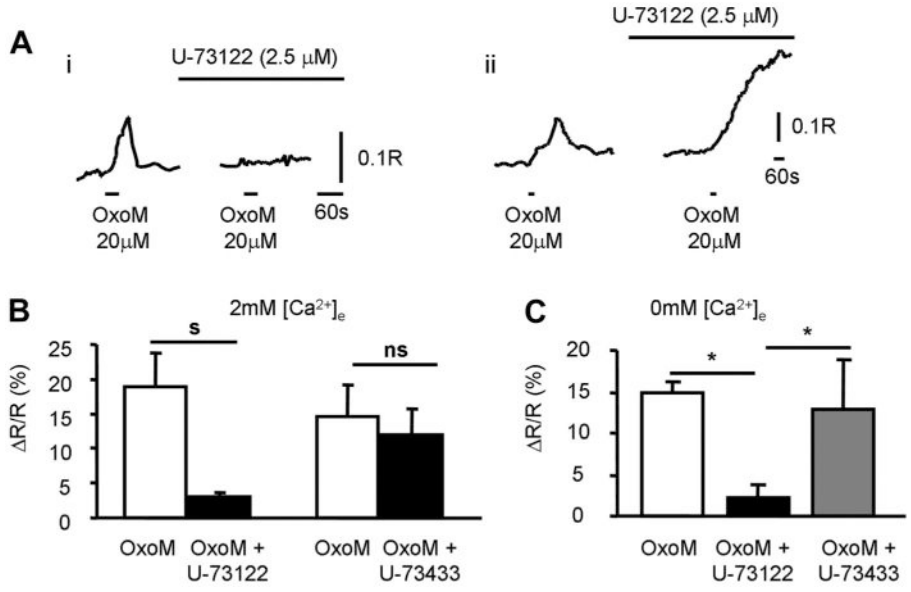

Fig. 7.

Intracellular pathways activated by mAChRs. *Ai*: example from a single urothelial cell of an OxoM (20 μM, 30-s application)-elicited response which was abolished in the presence of the PLC inhibitor U-73122 (2.5 μM). *Aii*: example from a single urothelial cell of an OxoM (20 μM, 30-s application)-elicited response which was not abolished in the presence of the PLC inhibitor U-73122 (2.5 μM) but it did not return to baseline. External [Ca^{2+}] was 2 mM in both examples. *B*: summary of the effects of PLC inhibitor U-73122 (n = 30 cells; 10 coverslips from 6 cultures) and the inactive analog U-73433 (n = 24 cells; 6 coverslips from 3 cultures) on OxoM-elicited responses in 2 mM external [Ca^{2+}]. s, ns indicate significant changes (s; $P < 0.05$) or not significant changes (ns; $P > 0.05$) tested with paired t-test. *C*: summary of OxoM-elicited responses from coverslips that were incubated in 0 mM external [Ca^{2+}] alone (white bar; n = 28 cells; 3 coverslips from 3 cultures), with the PLC inhibitor U-73122 (2.5 μM; black bar; n = 26 cells; 3 coverslips from 3 cultures), or with the inactive analog U-73433 (2.5 μM; gray bar; n = 23 cells; 3 coverslips from 3 cultures). *Significant changes ($P < 0.05$) tested with ANOVA followed by Bonferroni post hoc test.

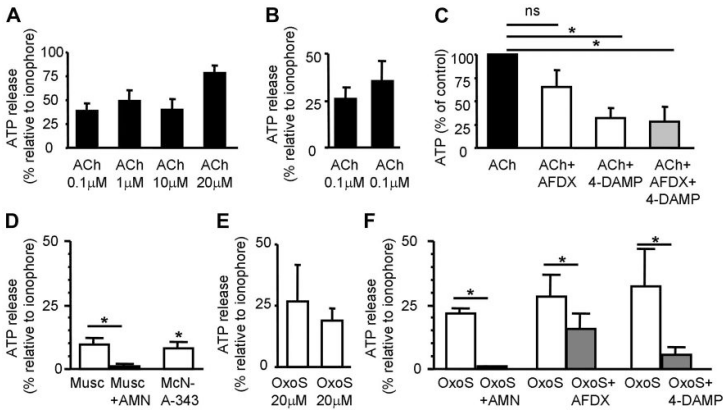

Fig. 8.

Activation of mAChR triggers release of ATP. *A*: ACh evokes release of ATP. Results are expressed as percentage of the ATP released by the ionophore ionomycin (5 μM); $n = 6, 3, 5, 3$ for each concentration, respectively. *B*: repeatability of ACh (0.1 μM)-evoked ATP release ($n = 3$). *C*: ACh (0.1 μM)-evoked ATP release is reduced by the M_2, M_3 mAChR antagonists AF-DX 116 (50 μM, $n = 3$), 4-DAMP (50 μM, $n = 3$), and by both antagonists applied together ($n = 4$). Cells were pretreated with antagonists 10–20 min before agonist application. *D*: muscarine (10 μM, $n = 4$) induces ATP release which is blocked by AMN (20 μM). The M1 agonist MCN-A-343 (1 μM, $n = 3$) induces ATP release. *E*: repeatability of oxotremorine sesquifumarate salt (OxoS; 20 μM)-evoked ATP release ($n = 6$). *F*: OxoS (20 μM)-evoked ATP release from cultured urothelial cells is greatly reduced by AMN (20 μM, $n = 3$) and only partially reduced by the M_2 and M_3 mAChR antagonists AF-DX 116 (1 μM, $n = 3$) and 4-DAMP, respectively. *Statistically significant differences ($P < 0.05$) tested with unpaired *t*-test (*C*) and paired *t*-test (*B*, *D*, *E*, *F*). *n* Represents number of coverslips.

Table 1

Primary and secondary antibodies

Primary and Secondary Antibodies	Dilution	Source
Monoclonal mouse anti-human, clone K_s20.8	1:500	Dako North America, Carpinteria, CA
Monoclonal mouse anti-human, clone E3	1:500	Dako North America
Donkey anti-mouse conjugated to Alexa-488	1:1,000	Invitrogen, Carlsbad, CA

Table 2

Drugs used in this study

Target	Drug Name	Abbreviation	Source
Nonselective mAChRs agonists	Muscarine	Musc	Sigma, St. Louis, MO
	Oxotremorine methiodide	OxoM	Sigma
	Oxotremorine sesquifumarate salt	OxoS	Sigma
	Acetylcholine	ACh	Sigma
Selective M_1 agonist	McN-A-343	McN-A-343	Sigma
Nonselective mAChR antagonist	Atropine methyl nitrate	AMN	Sigma
Selective M_2 antagonist	11-[[2-[(Diethylamino)methyl]-1-piperidinyl]acetyl]-5, 11-dihydro-6*H*-pyrido[2,3-b][1,4]benzodiazepin-6-one	AF-DX 116	Tocris, Ellisville, MI
Selective M_3 antagonist	4-diphenylacetoxy-N-methylpiperine	4-DAMP	Tocris
Nonselective purinergic receptor agonist	Adenosine 5′-triphosphate	ATP	Sigma
Nonselective purinergic receptor antagonist	4-[[4-formyl-5-hydroxy-6-methyl-3-[(phosphonooxy)methyl]-2-pyridinyl]azo]-1,3-benzenedisulfonic acid tetrasodium salt	PPADS	Sigma
PLC inhibitor	(1-[6-[((17β)-3-Methoxyestra-1,3,5[10]-trien-17-yl)amino]hexyl]-1H-pyrrole-2,5-dione)	U-73122	Sigma
Inactive analog of the PLC inhibitor	(1-[6-[((17β)-3-Methoxyestra-1,3,5[10]-trien-17-yl)amino]hexyl]-2,5-pyrrolidinedione)	U-73343	Sigma
Membrane-permeable diacylglycerol analog	1-Oleoyl-2-acetyl-*sn*-glycerol	OAG	Sigma
Calcium ionophore	Ionomycin	Ionomycin	Sigma

Table 3

Calcium responses elicited by OxoM

Concentration, M	Baseline, FAU*10^3	Peak, FAU*10^3	ΔR/R, %	% of Responding Cells	Coverslips (*n*) Cultures (*N*)
1×10^{-9}	490±22	540±24	10.26±2.16	5.2% (8/155)	*n* = 8; *N* = 4
1×10^{-8}	434±33	478±39	9.59±1.21	9.0% (11/122)	*n* = 8; *N* = 4
5×10^{-8}	433±43	498±33	15.25±2.21	12.5% (15/120)	*n* = 10; *N* = 5
1×10^{-7}	486±16	594±36	20.20±3.64	17.7% (34/192)	*n* = 12; *N* = 5
5×10^{-7}	424±23	502±63	18.41±3.79	23.4% (54/231)	*n* = 4; *N* = 3
1×10^{-6}	516±11	643±22	24.82±3.47	57.9% (55/95)	*n* = 9; *N* = 4
2×10^{-6}	447±12	554±28	22.76±4.42	25.8% (45/174)	*n* = 8; *N* = 4
5×10^{-6}	521±15	639±28	21.99±3.56	29.4% (45/160)	*n* = 7; *N* = 4
1×10^{-5}	513±17	601±25	15.92±1.87	51.1% (71/139)	*n* = 5; *N* = 4
2×10^{-5}	493±12	624±20	29.49±2.71	46.2% (54/117)	*n* = 11; *N* = 5

Values are means ± SE.